Adaptive Norm Selection for Regularized Image Restoration and Super-Resolution

Huanfeng Shen, *Senior Member, IEEE*, Li Peng, Linwei Yue, Qiangqiang Yuan, *Member, IEEE*, and Liangpei Zhang, *Senior Member, IEEE*

***Abstract*—In the commonly employed regularization models of image restoration and super-resolution (SR), the norm determination is often challenging. This paper proposes a method to adaptively determine the optimal norms for both fidelity term and regularization term in the (SR) restoration model. Inspired by a generalized likelihood ratio test, a piecewise function is proposed to solve the norm of the fidelity term. This function can find the stable norm value in a certain number of iterations, regardless of whether the noise type is Gaussian, impulse, or mixed. For the regularization norm, the main advantage of the proposed method is that it is locally adaptive. Specifically, it assigns different norms for different pixel locations, according to the local activity measured by a structure tensor metric. The proposed method was tested using different types of images. The experimental results and error analyses verify the efficacy of the method.**

***Index Terms*—Adaptive norm selection, image restoration, super-resolution (SR).**

I. Introduction

IMAGES captured by sensors are commonly corrupted by blurring and noise. Image restoration techniques aim to recover a high-quality image from its blurred and noisy measurement [1]–[4]. The conventional restoration techniques generally stay within a limited passband, and do not extend it. In contrast, super-resolution (SR) restoration is a technique that can break the inherent resolution limit, and produces a high-resolution image from low-resolution (LR) observations. It can therefore be considered as a second-generation problem of image restoration [5]. To address the typical inverse problem of image restoration and SR, a general imaging model can be represented as [6]

$$\boldsymbol{y}_k = \boldsymbol{D}_k\boldsymbol{B}_k\boldsymbol{M}_k\boldsymbol{z} + \boldsymbol{n}_k \tag{1}$$

where $\boldsymbol{y}_k$ is the kth observed image, and $\boldsymbol{z}$ is the desired image. $\boldsymbol{D}_k$, $\boldsymbol{B}_k$, and $\boldsymbol{M}_k$ are, respectively, the down-sampling, blurring, and motion operators, and $\boldsymbol{n}_k$ is the additive noise. When $\boldsymbol{D}_k$ and $\boldsymbol{M}_k$ are identity matrices, it is the model of a classical image restoration problem. For convenience of expression, (1) can be rewritten as (2) by substituting the product of $\boldsymbol{D}_k$, $\boldsymbol{B}_k$, and $\boldsymbol{M}_k$ by $\boldsymbol{A}$, and putting all the observed images together $\boldsymbol{y} = [\boldsymbol{y}_1^T, \boldsymbol{y}_2^T, \dots]^T$

$$\boldsymbol{y} = \boldsymbol{A}\boldsymbol{z} + \boldsymbol{n}. \tag{2}$$

Image restoration and SR have been extensively studied in recent decades. For a detailed review of these methods (see [5], [7]–[10]). Among the existing frameworks, the regularization method, which has been described from both algebraic and statistical perspectives [7], [11], is the most commonly used approach. The standard regularized solution of the inverse problem is the minimum of the functional [12]

$$L(\boldsymbol{z}) = \|\boldsymbol{y} - \boldsymbol{A}\boldsymbol{z}\|_p^p + \lambda\|\boldsymbol{\Gamma}(\boldsymbol{z})\|_q^q \tag{3}$$

where the first term is the data fidelity term, the second term is the regularization term, with $\boldsymbol{\Gamma}(\cdot)$ being a regularization function, and λ is the regularization parameter balancing these two terms.

For the data fidelity, the l_2 norm ($p = 2$)-based linear least squares term is widely used [6], [11], [13]–[15]. The main advantage of the l_2 norm problem is that it is easy to solve, and many efficient algorithms exist. However, the result solved by the l_2 model is only optimal when the noise is white Gaussian type [12]. Therefore, there has been a growing interest in using the l_1 norm with $p = 1$ [16]–[21]. It has been proven that the l_1 fidelity is more effective than the l_2 fidelity when the images contain impulse noise and outliers. Compared with the l_2 norm, however, the convergence rate of the l_1 norm is often much slower. Apart from the simplest gradient descent method [16], [17], [22], some other efficient approximation methods have also been developed [18]–[20], [23] for the

Manuscript received March 24, 2015 and accepted June 15, 2015. This work was supported in part by the National Natural Science Foundation of China under Grant 41422108, in part by the National Major Basic Research Development Program of China (973 Program) under Grant 2011CB707103, in part by the Program for Changjiang Scholars and Innovative Research Team in University under Grant IRT1278, and in part by the Hubei Natural Science Foundation under Grant 2011CDA096. This paper was recommended by Associate Editor. L. Shao.

H. Shen is with the School of Resource and Environmental Sciences, Wuhan University, Wuhan 430079, China, and also with the Collaborative Innovation Center of Geospatial Technology, Wuhan 430079, China (e-mail: shenhf@whu.edu.cn).

L. Peng is with the School of Resource and Environmental Sciences, Wuhan University, Wuhan 430079, China (e-mail: jiuguik@126.com).

L. Yue is with the State Key Laboratory of Information Engineering in Surveying, Mapping, and Remote Sensing, Wuhan University, Wuhan 430079, China (e-mail: yuelinwei2008@126.com).

Q. Yuan is with the School of Geodesy and Geomatics, Wuhan University, Wuhan 430079, China, and also with the Collaborative Innovation Center of Geospatial Technology, Wuhan 430079, China. (e-mail: qqyuan@sgg.whu.edu.cn).

L. Zhang is with the State Key Laboratory of Information Engineering in Surveying, Mapping, and Remote Sensing, Wuhan University, Wuhan 430079, China, and also with the Collaborative Innovation Center of Geospatial Technology. (e-mail: zlp62@whu.edu.cn).

Color versions of one or more of the figures in this paper are available online at http://ieeexplore.ieee.org.

Digital Object Identifier 10.1109/TCYB.2015.2446755

l_1 optimization. For complicated types of noise and/or model error, however, both l_1 and l_2 norms have their advantages and disadvantages. Some researchers have therefore employed an $l_1 - l_2$ hybrid model for the fidelity term [24]–[26].

To constrain the solution space of the ill-posed problems of image restoration and SR, a number of different regularization methods have been proposed. Traditional models, such as the Tikhonov [27] and Gauss–Markov [28] types, use the l_2 norm with $q = 2$. A common criticism of these regularization methods is that the sharp edges and detailed information in the estimates tend to be overly smoothed [29]. To effectively preserve the edge and detailed information in the image, some edge-preserving regularization models have been employed in image (SR) restoration. The l_1 norm ($q = 1$)-based total variation (TV) regularization [11], [29] and its derived versions such as bilateral TV [16], [17] are the most widely used edge-preserving models. Using the TV methods, however, there is often a tradeoff between the preservation of detailed information in the edge regions and the avoidance of staircase effects in the smooth regions [30], [31]. The Huber–Markov regularization [13], [22], [32], [33] can theoretically relieve this tradeoff to some degree because its energy function is a mixed mode of the l_1 and l_2 norms. To more effectively consider this problem, some researchers have considered an adaptive norm ($q = 1$ or $q = 2$), according to the determined image structures (smooth regions or edges) [12], [31].

In summary, whether for the fidelity term or the regularization term, neither the l_1 norm nor the l_2 norm is optimal in many cases. The optimal fidelity norm is mainly affected by the type of noise and/or model error, and the best value for the regularization norm is greatly related to the image structures. The combination of l_1 and l_2 norms [12], [24]–[26], [31], [34] may produce some new difficulties, such as the weight determination and efficient optimization. This paper proposes a method to adaptively determine the optimal norms as arbitrary values in the interval [1, 2] for both fidelity term and regularization term in the (SR) restoration model. The main contributions are twofold. First, the optimal norm of the data fidelity can be adaptively estimated in a Gaussian/impulse case using the statistical information. This solves a significant problem in image restoration/SR. Second, we assign locally adaptive norm values for the regularization according to the spatial structure. By employing the spatially adaptive norm, the proposed regularization can achieve a good balance between noise suppression and edge preservation. Combining the two parts into a joint framework, we believe that the proposed method provides a new insight into the common difficulty of norm selection in image inverse problems.

II. Restoration Framework and Optimization Method

A. Restoration Framework

By selecting $\mathbf{\Gamma}(\cdot)$ in (3) as a gradient operator, a general TV minimization functional is [35]

$$E(z) = \|\boldsymbol{y} - \boldsymbol{A}\boldsymbol{z}\|_p^p + \lambda \left\| \sqrt{(\nabla^x \boldsymbol{z})^2 + (\nabla^y \boldsymbol{z})^2 + \beta} \right\|_q^q \quad (4)$$

where ∇^x and ∇^y are linear operators corresponding to the horizontal and vertical first-order differences, and β is a small positive parameter which ensures differentiability.

Although the p and q norms in (4) can be arbitrary values in the interval (0, 2], the effects of the image structures are not considered. It has been proven that edge regions prefer a lower value of q to preserve the detailed information, and smooth regions require a larger value of q to avoid artifacts such as staircase effects [12], [31]. Taking this into account, this paper proposes to use a more general restoration model

$$E(z) = \|\boldsymbol{y} - \boldsymbol{A}\boldsymbol{z}\|_p^p + \lambda \sum_{i,j} \left\| \sqrt{\left(\nabla_{i,j}^x z\right)^2 + \left(\nabla_{i,j}^y z\right)^2 + \beta} \right\|_{q_{i,j}}^{q_{i,j}} \quad (5)$$

where $q_{i,j}$ is the norm at pixel location (i, j).

B. Optimization Method

Since p and $q_{i,j}$ in (5) are arbitrary values in an interval, the conventional linear optimization methods cannot be directly employed. This paper employs the iteratively reweighted least squares (IRLS) method [35], [36] and the lagged diffusivity fixed point iteration (LDFPI) [11], [37] for the linearization of the fidelity term and the regularization term, respectively. Both of the methods implement the approximation based on iterative procedures. In general, the IRLS method converts the l_p function into an l_2 minimization problem at each iteration. Concretely, at iteration $n+1$, the solution z_{n+1} is the minimizer of

$$E_{n+1}(z) = \left\| \boldsymbol{W}_{z_n}^{1/2} (\boldsymbol{y} - \boldsymbol{A}\boldsymbol{z}) \right\|_2^2 + \lambda \sum_{i,j} \left\| \sqrt{\left(\nabla_{i,j}^x z\right)^2 + \left(\nabla_{i,j}^y z\right)^2 + \beta} \right\|_{q_{i,j}}^{q_{i,j}}. \quad (6)$$

In this equation, $\boldsymbol{W}_{z_n}$ is defined as [35]

$$\boldsymbol{W}_{z_n} = diag(\tau_\varepsilon(\boldsymbol{y} - \boldsymbol{A}\boldsymbol{z}_n)) \quad (7)$$

with

$$\tau_\varepsilon(x) = \begin{cases} |x|^{p-2} & \text{if } |x| > \varepsilon \\ \varepsilon^{p-2} & \text{if } |x| \le \varepsilon \end{cases} \quad (8)$$

where ε is a small positive number to guarantee global convergence, which we fix as 10^{-5} in this paper.

A concise IRLS minimization method for the regularization term in model (4) is also proposed in [35]. In order to deal with the more complicated model (5) and obtain an accurate difference approximation, the LDFPI strategy [11], [37] is employed. After converting the data fidelity term into the l_2 norm, the Euler–Lagrange equation for the energy function in (6) is given by the following system:

$$\nabla E_{n+1}(z) = \boldsymbol{A}^T \boldsymbol{W}_{z_n} (\boldsymbol{A}\boldsymbol{z} - \boldsymbol{y}) - \lambda \boldsymbol{L}_z \boldsymbol{z} = 0 \quad (9)$$

where $\boldsymbol{L}_z$ is the matrix form of a central difference approximation of the differential operator

$$q_{i,j} \nabla \cdot \left(\nabla \Big/ \left(\sqrt{\left(\nabla_{i,j}^x z\right)^2 + \left(\nabla_{i,j}^y z\right)^2 + \beta} \right)^{2-q_{i,j}} \right) \quad (10)$$

Where $\nabla\cdot$ is the divergence operator. Clearly, (10) is a nonlinear operator, which leads to difficulties in the solution. The LDFPI method [11], [37] consists of linearizing the nonlinear differential term by lagging the diffusion coefficient one iteration behind. Thus, z_{n+1} is obtained as the solution to the linear equation

$$\left(\boldsymbol{A}^T\boldsymbol{W}_{z_n}\boldsymbol{A}-\lambda\boldsymbol{L}_{z_n}\right)z_{n+1}=\boldsymbol{A}^T\boldsymbol{W}_{z_n}\boldsymbol{y}. \tag{11}$$

Since a central difference approximation is used, $-\boldsymbol{L}_{z_n}$ is symmetric and positive semi-definite. A detailed mathematical derivation can be found in [37]. To solve the above equation, this paper uses the factorized banded inverse preconditioner method [38].

III. Adaptive Method of Norm Selection

In this section, two functions are proposed for the adaptive selection of the arbitrary norm values in a confidence interval. The p and $q_{i,j}$ values are found in an alternate manner with the desired image solved based on (11). In general, there is a broad consensus that it is unnecessary to set p or $q_{i,j}$ greater than 2. On the other hand, few references consider a norm of less than 1 in the standard restoration and SR models (except for the sparse and/or compressed sensing frameworks). Our experimental results also indicate that $p>2$ or $q_{i,j}<1$ are not necessary to improve the robustness of the restoration model. In this paper, therefore, we restrict the interval to [1], [2] for both p and $q_{i,j}$.

A. Adaptive Selection of the Fidelity Norm p

It is known that the optimal norm p is closely related to the distribution of the N-dimensional noise vector $\boldsymbol{n}$ in (2). In the image processing field, the Gaussian type noise is the most commonly assumed because it is usually generated in image acquisition [39]. In many applications, practical systems can suffer from outliers, which are typically caused by malfunctioning arrays in camera sensors, faulty memory locations in hardware, or transmission in a noisy channel [40]. In the image SR problem, there is often a special type of outliers existing because some pixels in one image may be unobservable in the other images. The outliers are commonly assumed to be impulse noise [41], [42] and can be modeled using a Laplacian distribution [43]. Therefore, we employ the Gaussian and Laplacian distributions, which are the two major candidates in the inverse problem of image processing [16], [26]. They are, respectively, defined as

$$P_G(\boldsymbol{n})=\frac{1}{\left(\sqrt{2\pi}\sigma_G\right)^N}\exp\left\{-\sum_{i=1}^{N}(n_i-\mu_G)^2\Big/2\sigma_G^2\right\} \tag{12}$$

$$P_L(\boldsymbol{n})=\frac{1}{(2\sigma_L)^N}\exp\left\{-\sum_{i=1}^{N}|n_i-\mu_L|\Big/\sigma_L\right\} \tag{13}$$

where n_i is the ith element of the noise vector $\boldsymbol{n}$. The maximum likelihood of the model parameters μ_G, σ_G, μ_L, and σ_L can be computed from the data as follows:

$$\begin{cases}\hat{\mu}_G=\text{mean}(\boldsymbol{n}),\ \hat{\sigma}_G=\sqrt{\sum_{i=1}^{N}(n_i-\mu_G)^2\Big/N}\\ \hat{\mu}_L=\text{median}(\boldsymbol{n}),\ \hat{\sigma}_L=\sum_{i=1}^{N}|n_i-\mu_L|\Big/N.\end{cases} \tag{14}$$

(a) (b) (c) (d)

Fig. 1. Images used to set up the function between p and γ. (a) *Foreman* image. (b) *Lena* image. (c) *Barbara* image. (d) *Peppers* image.

In general, the Gaussian and Laplacian distributions, respectively, correspond to the l_2 and l_1 norms [16], [26]. This means that when $\boldsymbol{n}$ is Gaussian distributed, $p=2$ is preferable; and when $\boldsymbol{n}$ is a Laplacian type, which is more accurate for modeling the impulse noise and/or outliers, $p=1$ is optimal. In image restoration and SR, however, the distribution of $\boldsymbol{n}$ is often neither rigid Gaussian nor rigid Laplacian, but a combination of them [26]. In this case, the optimal norm p should be greater than 1 and less than 2. In order to obtain robust models in the processing of noisy data, some studies employ the framework of a generalized Gaussian distribution (GGD), and look for estimators for a shape parameter in the GGD model, which has an identical attribute to the parameter p [44].

Inspired by [16] and [26], this paper determines the optimal p based on a generalized likelihood ratio test (GLRT). In order to determine the type of noise model, GLRT can be used to judge whether the following inequality is satisfied:

$$\frac{P_G\left(\boldsymbol{n};\hat{\mu}_G,\hat{\sigma}_G\right)}{P_L\left(\boldsymbol{n};\hat{\mu}_L,\hat{\sigma}_L\right)}>\xi \tag{15}$$

where ξ is a threshold. The parameter ξ is often selected as 1 [16], [26]. Substituting (12), (13), and (14) into (15), using $\xi=1$, and defining $\gamma=\hat{\sigma}_L/\hat{\sigma}_G$, it can be simplified as

$$\gamma>\left(\frac{\pi}{2e}\right)^{0.5}\approx 0.7602. \tag{16}$$

That is, if the ratio $\gamma=\hat{\sigma}_L/\hat{\sigma}_G$ is larger than 0.7602, then P_G (Gaussian, l_2 norm) is a more accurate model than P_L (Laplacian, l_1 norm), and vice versa.

Using the above inequality, we can only determine whether the l_1 norm or l_2 norm is better. Our objective is to find an optimal norm value p in the interval [1], [2]. It is obvious that this value should be closely related to the parameter γ, which is an indicator of the approximation degree of the l_1 or l_2 norms, according to the GLRT. To validate this, four standard test images (*Foreman*, *Lena*, *Barbara*, and *Peppers*) (as shown in Fig. 1) are used to produce a certain amount of $p-\gamma$ points. The detailed steps are as follows.

1) Degrade the images using the motion, blurring, and down-sampling operators, as shown in (1).
2) Add noise to the images produced in step 1), and for each image, nine different combinations of Gaussian and impulse noise (as shown in Table I) are, respectively, tested.
3) For each noise combination, compute the noise vector $\hat{n}=\boldsymbol{y}-\boldsymbol{A}\boldsymbol{z}$ based on (2), compute $\hat{\sigma}_L$ and $\hat{\sigma}_G$ based on (14), and then obtain the corresponding γ value using $\gamma=\hat{\sigma}_L/\hat{\sigma}_G$.

TABLE I
NINE NOISE COMBINATIONS IN THE $p-\gamma$ FITTING

	1	2	3	4	5	6	7	8	9
Gaussian variance	0	0.0001	0.0002	0.0005	0.001	0.001	0.001	0.001	0.001
Impulse density	0.01	0.01	0.01	0.01	0.01	0.005	0.002	0.0005	0

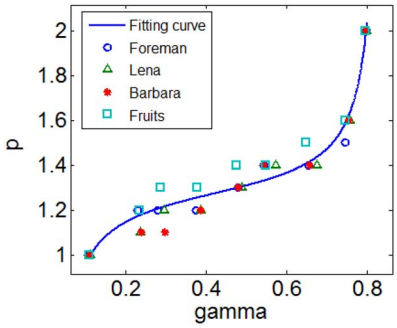

Fig. 2. $p-\gamma$ points and their fitted curve.

4) For each noise combination, adjust p from 1 to 2 (at an increment of 0.1) to implement the (SR) restoration algorithm described in Section II with the standard TV regularization ($q=1$).
5) The original images are used as the reference to evaluate the resulting images, and to seek the optimal p for each γ.

After the above procedure, four series of $p-\gamma$ points are produced, as shown in Fig. 2. It can be seen that the four series of points have very similar trends. Through a large number of trials on different images, we found that this feature is consistent. This forms the basis for us to look for a function by implementing curve fitting, and to apply this function for the determination of p during the image (SR) restoration process.

The $p-\gamma$ function should have the following two basic properties: 1) the maximum of p is 2, and the minimum is 1 and 2) p is monotonically increasing with γ. According to the spatial distribution of these points, we assume the following tangent function:

$$p = a\tan(b\gamma + c) + d \tag{17}$$

where a, b, c, and d are the model parameters. It is overdetermined to solve these four parameters using the available $p-\gamma$ points. The solved values are

$$\begin{cases} a = 0.115 & b = 3.777 \\ c = -1.601 & d = 1.276. \end{cases} \tag{18}$$

The fitted curve is also illustrated in Fig. 2. Considering $p \in [1, 2]$, the piecewise function of p is given as

$$p = \begin{cases} 1 & 0 < \gamma \le 0.112 \\ a\tan(b\gamma + c) + d & 0.112 < \gamma \le 0.798 \\ 2 & 0.798 < \gamma < 1 \end{cases} \tag{19}$$

where the parameters of 0.112 and 0.798 are the corresponding γ values when p was, respectively, solved as 1 and 2, based on (17).

It should be noted that although the four model parameters may be different, based on the different test images, the obtained curves are very close. The results are also not sensitive to the solved norms with the slightly differing parameters. This is tested in the experiment part by performing the proposed method on images which are different to the four test ones. Another issue is the computation of γ, which needs the ideal image z according to step 3). In real applications, however, z is what we want to solve, and is unknown. We solve this problem using the following strategy: 1) in the first iteration, z is substituted by the initial guess and 2) in the following iterations, it is substituted by the partially reconstructed image. Although there may be considerable bias in the first few iteration steps, this can be greatly relieved when the partially reconstructed image approaches the ideal image in the next iterations.

B. Adaptive Selection of the Regularization Norm $q_{i,j}$

As mentioned before, a larger regularization norm should be set to suppress noise and artifacts for flat-area pixels. In contrast, for edge-area pixels, a smaller norm should be set to preserve the detailed information. Therefore, a local activity indicator is needed to determine whether the pixels belong to smooth regions or edges. This paper employs a structure tensor indicator, which was first proposed in [45], and has been widely used and expanded upon in [31] and [46]–[49]. It has been proven that this indicator is a powerful tool for the discrimination of edges from flat regions. For each pixel, the structure tensor matrix is defined as

$$S_{i,j} = K * \left[\left(\nabla_{i,j} z\right) \left(\nabla_{i,j} z\right)^T \right] \tag{20}$$

where $\nabla_{i,j} z = [\nabla^x_{i,j} z, \nabla^y_{i,j} z]^T$, with $\nabla^x_{i,j} z$ and $\nabla^y_{i,j} z$ being the gradient information in the horizontal and vertical directions at pixel (i, j). K is a smooth operator, which is usually defined as a Gaussian kernel. Here we use a 5×5 equal-weight blur kernel, i.e., the variance is infinite. The symbol "*" means convolution. In order to determine the spatial property (local activity) of each pixel more accurately, a block containing the neighbored pixels is often needed. The structure tensor for the block whose central pixel locates at (i, j) can be defined as

$$S^b_{i,j} = \frac{1}{(2R+1)^2} \sum_{k=i-R}^{i+R} \sum_{l=j-R}^{j+R} S_{k,l} \tag{21}$$

where $2R+1$ is the block size in both horizontal and vertical dimensions. We select a size of 5×5 (R=2) for the block in this paper. Based on the structure tensor matrix, the local activity of the central pixel can be defined as

$$\delta_{i,j} = |\kappa_1| + |\kappa_2| \tag{22}$$

where κ_1 and κ_2 are the two eigenvalues of the structure tensor matrix $S^b_{i,j}$. The larger the parameter $\delta_{i,j}$ is, the more possible it is that the pixel belongs to an edge region.

Since $\delta_{i,j}$ is selected as the local activity metric, the regularization norm $q_{i,j}$ can be solved by designing a functional as $q = f(\delta)$. In order to ensure $q_{i,j} \in [1, 2]$, we define

$$q_{i,j} = 2 - t_{i,j} \tag{23}$$

where $t_{i,j}$ is a projection of the structure tensor $\delta_{i,j}$ to the scope of the interval [0, 1]. Because $\delta_{i,j}$ tends to be larger in the edge regions, $t_{i,j}$ should be directly proportional to $\delta_{i,j}$ to ensure that the edge regions are assigned small norms. In this paper, the following function is designed:

$$t_{i,j} = \frac{\log \delta_{i,j} - \log \delta_{\min}}{\log \delta_{\max} - \log \delta_{\min} + \vartheta} \tag{24}$$

where $\delta_{\min}$ and $\delta_{\max}$ are, respectively, the minimum and maximum of δ in all the locations of the image. Since the $\delta_{i,j}$ values often have considerable differences, the logarithm function $\log(\cdot)$ is used to narrow the values to a reasonable range. If the value of $\delta_{i,j}$ is less than 1 at any pixel, we replace it with 1 to ensure $t_{i,j}$ is larger than or equal to 0. The parameter ϑ is a small parameter to prevent the dominator being 0, and we fix it as 10^{-5} in this paper.

Using (23) and (24), each pixel in the image can be given a value for the regularization norm, and the minimum and maximum values are, respectively, 1 and 2. In a practical situation, however, the overall distribution of the image structure still has a considerable effect on the norm selection. To satisfy this law, we rewrite (23) as (25)

$$q_{i,j} = 2 - \left(t_{i,j}\right)^{\alpha}. \tag{25}$$

In (25), α is a shape controller parameter. If $\alpha = 0$, all the $q_{i,j}$ values are equal to 1, and the standard l_1-based TV model can be obtained; if α is positive infinity, the l_2 regularization can be approached. In fact, most natural images are more suited to be fit with smaller norms for the regularization term. Therefore, the scope of α commonly falls into the interval (0, 1]. The adaptive determination of α is another more difficult issue. However, we use a compromised parameter setting by fixing α as 0.5 in this paper. Under this circumstance, the proposed method still has advantages over the other regularizations, which is validated in the experiment part.

In conclusion, the adaptive norm restoration/SR framework can be generalized into a joint framework. The flowchart of the proposed algorithm is shown in Fig. 3.

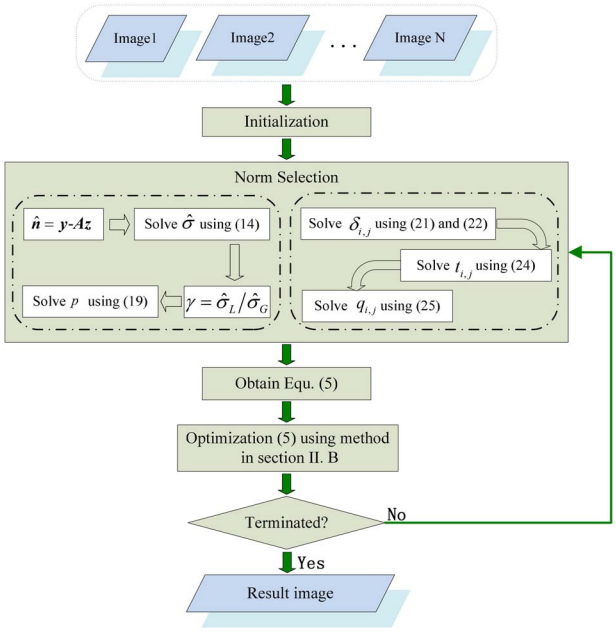

Fig. 3. Flowchart of the proposed method.

(a) (b)

Fig. 4. Images used in the validation of the p function. (a) *Lena* and (b) *Satellite* images.

IV. Experiments

A. Validation of the Adaptive p Norm

The first experiment for the validation of the p function was performed for classical image restoration. The *Lena* and *Satellite* images shown in Fig. 4 were used. The original images were first blurred by different convolution kernels, which were, respectively, 3×3 (standard deviation = 1), 5×5 (standard deviation = 1.5), and 7×7 (standard deviation = 2). The blurred images were then, respectively, contaminated by Gaussian noise with a normalized variance of 0.001, impulse noise with a density of 0.01, and a mixed mode of the two noise types. The regularization norm was set as 1, i.e., a standard TV model was employed. In the traditional manual method, 11 equally spaced candidate values were fixed in the interval of [1, 2] for the fidelity norm. The norm value that produced the highest peak signal-to-noise ratio (PSNR) was regarded as the optimal one. The proposed adaptive method was implemented to test how close its results were to the optimal results in the manual method.

The quantitative evaluation results are shown in Table II. PSNR (dB) and p values in the validation of the adaptive norm of the fidelity term (restoration experiment). Here, it can be seen that the optimal norms of the Gaussian and impulse noise cases are, respectively, 2.0 and 1.0 in all the scenarios. Most of the optimal norms of the mixed noise cases are 1.3, with only one exception of 1.4. On the whole, the norm values adaptively computed with the proposed method are very close to the optimal values. Only in two cases are the deviations greater than 0.05, which are highlighted in bold in Table II. PSNR (dB) and p values in the validation of the adaptive norm of the fidelity term (restoration experiment). The PSNR values of the adaptive method are also very close to the optimal ones, even in the two highlighted cases. Therefore, the adaptive method for the fidelity norm is validated as being effective in this experiment. The restored *Lena* images of the l_1, l_2, and the proposed l_{a_p} (adaptive norm for the p function) methods in one mixed noise case are illustrated in Fig. 5. Here, it can be seen that the l_2 norm gives the worst results because it cannot completely remove the impulse noise. The visual quality of the l_1 norm is superior to the l_2 norm due to its robustness to impulse noise.

TABLE II
PSNR (dB) AND p VALUES IN THE VALIDATION OF THE ADAPTIVE NORM OF THE FIDELITY TERM (RESTORATION EXPERIMENT)

Images Blur/noise		Lena				Satellite			
		p		PSNR		p		PSNR	
		Opt.	Adap.	Opt.	Adap.	Opt.	Adap.	Opt.	Adap.
3×3	Gaussian	2.0	1.91	29.466	29.462	**2.0**	**1.80**	**26.130**	**26.114**
	Impulse	1.0	1.00	35.900	35.892	1.0	1.00	34.753	34.743
	Mixed	1.3	1.29	29.100	29.098	1.3	1.27	25.697	25.697
5×5	Gaussian	2.0	1.99	27.799	27.798	2.0	1.96	23.424	23.423
	Impulse	1.0	1.00	31.922	31.921	1.0	1.00	29.073	29.074
	Mixed	1.3	1.30	27.600	27.600	1.3	1.29	23.177	23.175
7×7	Gaussian	2.0	2.00	26.655	26.656	2.0	2.00	21.702	21.703
	Impulse	1.0	1.00	29.827	29.830	1.0	1.00	26.336	26.339
	Mixed	1.3	1.30	26.450	26.450	**1.4**	**1.29**	**21.635**	**21.624**

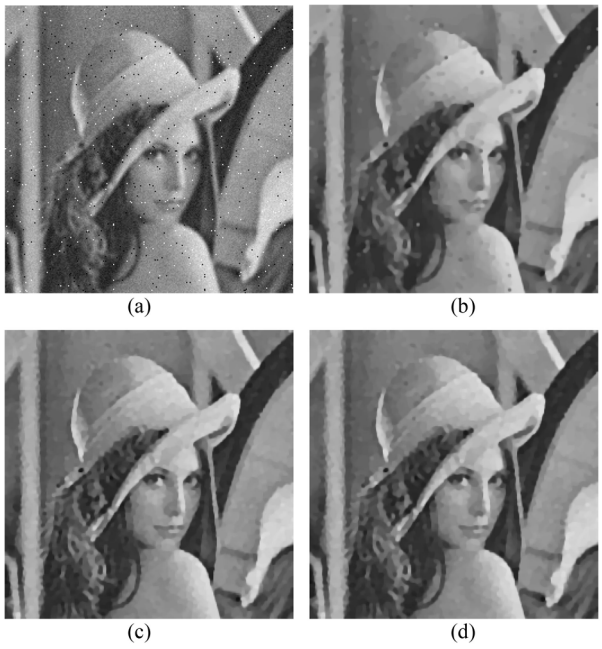

Fig. 5. Restoration results of the *Lena* image in the mixed noise case (5×5 blur, standard deviation = 1.5). (a) Degraded image. Result of the (b) l_2 norm, (c) l_1 norm and (d) Proposed adaptive norm.

The proposed l_{a_p} norm produces more desirable results than both l_1 norm and l_2 norm because it can effectively deal with Gaussian and impulse noise simultaneously.

The second experiment was performed for SR reconstruction. The original images were first down-sampled by a factor of 2. Thus, in each case four LR images were obtained, with the translational shifts being (0, 0), (0, 0.5), (0.5, 0), and (0.5, 0.5). The down-sampled images were then contaminated by different types of noise. Since we are mainly concerned with the SR performance, no blur was considered in this experiment. In order to validate the robustness more effectively, one impulse noise mode, one Gaussian noise mode, and six mixture modes were tested. The corresponding relationships between the variances of the Gaussian noise and the densities of the impulse noise were: impulse (0, 0.01), Mixed-1 (0.001, 0.01), Mixed-2 (0.003, 0.03), Mixed-3 (0.005, 0.01), Mixed-4 (0.007, 0.007), Mixed-5 (0.009, 0.005), Mixed-6 (0.01, 0.003), and Gaussian (0.002, 0).

TABLE III
PSNR (dB) AND P VALUES IN THE VALIDATION OF THE ADAPTIVE NORM OF THE FIDELITY TERM (SR EXPERIMENT)

Images	Lena				Satellite			
	p		PSNR		p		PSNR	
Noise	Opt.	Adap.	Opt.	Adap.	Opt.	Adap.	Opt.	Adap.
Impulse	1.0	1.00	40.809	40.809	1.0	1.00	40.597	40.510
Mixed-1	1.3	1.28	30.179	30.183	1.2	1.26	27.538	27.553
Mixed-2	1.3	1.32	28.318	28.305	1.2	1.30	25.035	24.993
Mixed-3	1.4	1.43	27.894	27.897	1.4	1.39	24.462	24.461
Mixed-4	1.6	1.54	27.374	27.381	1.5	1.49	23.949	23.949
Mixed-5	1.6	1.65	27.093	27.095	1.6	1.59	23.548	23.547
Mixed-6	1.7	1.76	26.955	26.952	1.7	1.73	23.390	23.387
Gaussian	2.0	1.98	29.741	29.739	2.0	2.0	24.400	24.400

Table III shows the optimal and solved norm and PSNR values. The changes of PSNR versus the fidelity norm p in the different noise modes are charted in Fig. 6, with the Satellite image as an example. From Table III and Fig. 6, it can be seen that as long as the relative proportion of Gaussian noise is larger (or the relative proportion of impulse noise is smaller), the optimal norm value p increases, which agrees with the analysis in Section III-A. In all the noise modes, in terms of both norm and PSNR measurements, the proposed method obtains very similar results to the optimal values obtained in the manual method. This again validates that the proposed method has a good performance when seeking the optimal fidelity norm. Some results are shown in Fig. 7, from which the superiority of the proposed l_{a_p} norm method over the l_1 norm and l_2 norm-based methods can be embodied from a visual perspective. Fig. 8 illustrates the change of the solved p with the increase in the iteration number. Here, it can be seen that, in the first few iterations, the p value tends to be inaccurate because it is solved using a partly reconstructed image. After a certain number of iterations, however, it converges to a reasonable value.

B. Validation of the Adaptive q Norm

A basic characteristic of the proposed method for the regularization term is the use of the locally adaptive function, as shown in (5). To validate its advantage, both image restoration and SR reconstruction were implemented. In the restoration experiment, again, three blurs of 3×3 (standard deviation = 1), 5×5 (standard deviation = 1.5), and 7×7 (standard deviation = 2) were considered. In the SR experiment, the down-sampling factor was chosen as 2, no blur was added, and three Gaussian noise modes with variance = 0 (noiseless), variance = 0.001, and variance = 0.002 were considered. It should be noted that, since the suppression of impulse noise mainly depends on the selection of p norm, only experiments on images contaminated by Gaussian noise

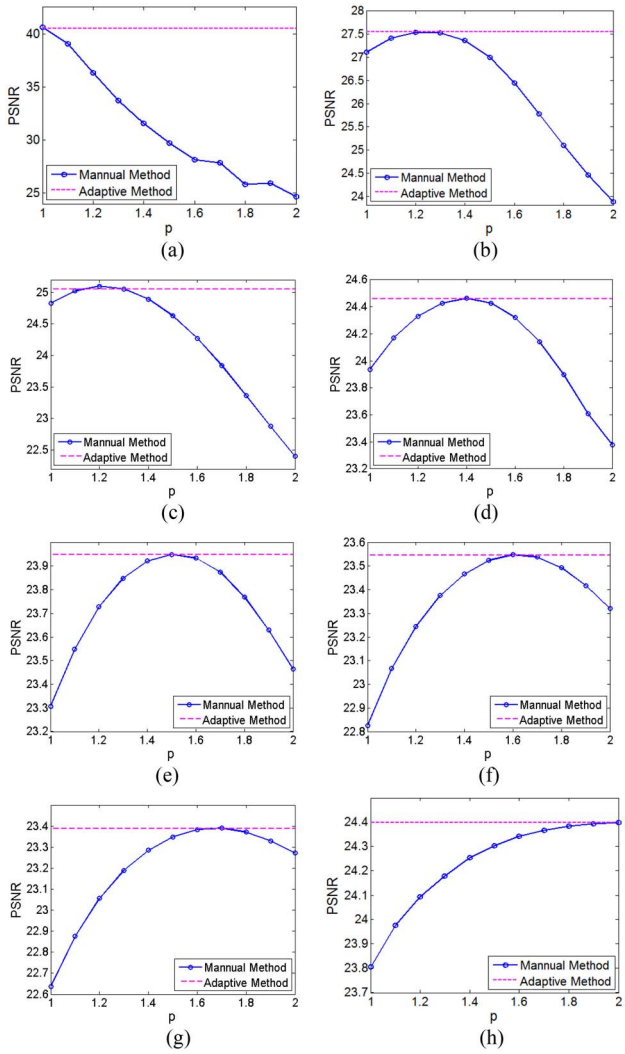

Fig. 6. PSNR values versus the fidelity norm p in the SR reconstruction (Satellite image). (a) Impulse. (b) Mixed-1. (c) Mixed-2. (d) Mixed-3. (e) Mixed-4. (f) Mixed-5. (g) Mixed-6. (h) Gaussian.

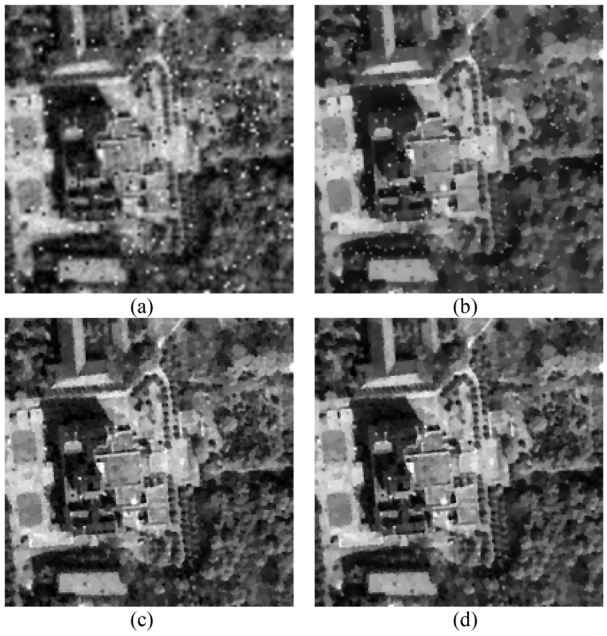

Fig. 7. SR results of the Satellite image for the validation of the adaptive norm of the fidelity term in Mixed-2 case (Gaussian variance = 0.003, impulse density = 0.03). (a) Degraded image. (b) l_2 norm. (c) l_1 norm. (d) Proposed $l_{a,p}$ norm.

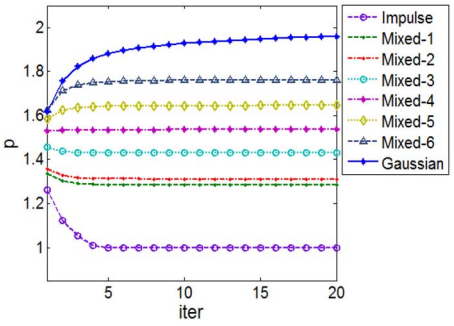

Fig. 8. Convergence performance of the p function in the different noise cases (Satellite image).

are given here for saving the space. To make a comparative analysis, the iteratively reweighted TV (IRTV) [35] method, the adaptive norm algorithm (ANA) [12], and the spatially weighted TV (SWTV) [30] method were also implemented. Among these methods, the IRTV method is based on a standard l_1 norm TV model; the ANA method employs hybrid l_1 and l_2 norms, respectively, for the flat regions and the edge regions in the image; and the SWTV method locally estimates the regularization parameter.

The PSNR evaluation results of the restoration and SR experiments are, respectively, shown in Tables IV and V. Because of the consideration of adaptive regularization, the ANA method, the SWTV method, and the proposed $l_{a,q}$ norm method all show improvements over the standard TV method (IRTV). For both restoration and SR reconstruction, the proposed method produces the highest PSNR values. For the Satellite image in particular, the PSNR value has about a 1 dB increase over the IRTV method in the noiseless cases.

To give a visual evaluation of the proposed locally adaptive regularization model, Fig. 9 shows the *Lena* images and

TABLE IV
PSNR (dB) RESULTS IN THE VALIDATION OF THE ADAPTIVE NORM OF THE $l_{a,q}$ REGULARIZATION (RESTORATION EXPERIMENT)

Image	Blur	IRTV	ANA	SWTV	Proposed
Lena	3×3	36.603	36.657	36.694	36.928
	5×5	32.447	32.524	32.639	32.815
	7×7	30.283	30.329	30.481	30.629
Satellite	3×3	35.407	35.694	35.719	36.244
	5×5	29.640	29.741	29.973	30.218
	7×7	26.865	26.902	27.134	27.258

detailed regions in the SR experiments (variance = 0.002). Here, it can be seen that the IRTV method results in staircase effects in the smooth regions. This is the main disadvantage of the standard TV model. The ANA method deals with the staircase problem very well by performing the l_2 norm on smooth regions; however, it often leads to an over-smoothing problem. Although the SWTV method produces higher PSNR values than ANA, it has no obvious advantage from the visual perspective. The proposed $l_{a,q}$ regularization outperforms the

TABLE V
PSNR (dB) Results in the Validation of the Adaptive Norm of the $l_{a,q}$ Regularization (SR Experiment)

Image		IRTV	ANA	SWTV	Proposed
Lena	noiseless	42.109	42.161	42.135	42.329
	variance=0.001	30.628	30.713	30.791	31.023
	variance=0.002	29.601	29.694	29.745	29.984
Satellite	noiseless	42.120	42.160	42.298	43.092
	variance=0.001	28.028	28.030	28.340	28.463
	variance=0.002	24.141	24.190	24.317	24.540

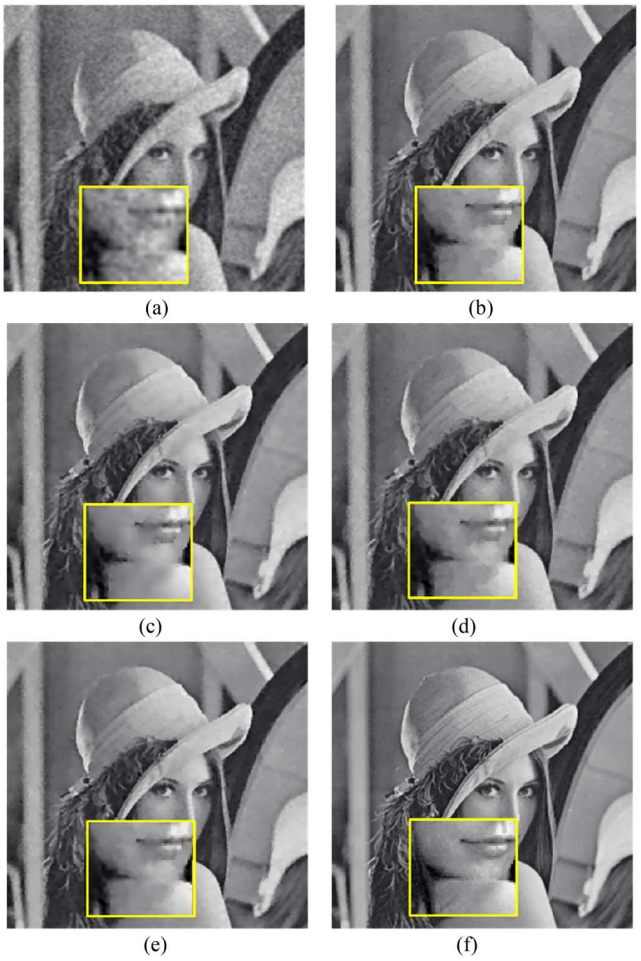

Fig. 9. SR results of the *Lena* image for the validation of the locally adaptive $l_{a,q}$ regularization. (a) Degraded image. (b) IRTV. (c) ANA. (d) SWTV. (e) Proposed $l_{a,q}$ regularization. (f) Original image.

other methods in terms of both quantitative evaluation and visual inspection.

C. Joint Validation of the Adaptive p and q Norms

After independent validation of the adaptive p and q norms, here we give a further joint validation of them. The proposed adaptive method was first compared with the manual method which interactively adjusts p and q for model (4). We manually adjusted p and q from 1 to 2 at increments of 0.1, respectively, to obtain 11×11 p-q pairs. The SR experiment performed on the *Lena* and *Satellite* images contaminated by mixed noise

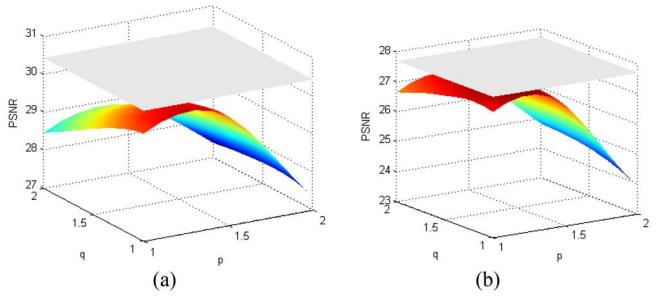

Fig. 10. Comparison between the manual method (curved surface) and the proposed adaptive method (plane surface). (a) *Lena* and (b) *Satellite* images.

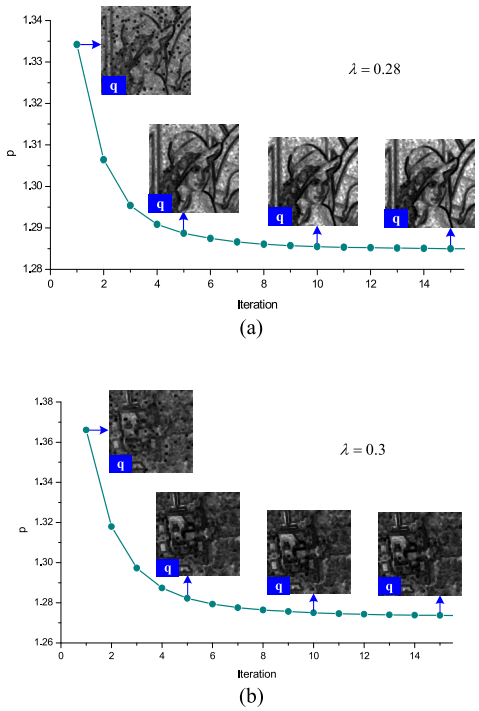

Fig. 11. Norm values versus the iteration number (a linear stretching is performed when mapping q values). (a) *Lena* and (b) *Satellite* images.

(Gaussian variance $= 0.001$, impulse density $= 0.01$) is illustrated in Fig. 10. The same parameter setting was adopted as the previous SR experiment. The curved surface represents the PSNR values of the resulting images using all the 11×11 pairs of p and q. The plane surface is the PSNR of the proposed adaptive method. It can be seen that the plane surface is completely above the curved surface, which confirms the advantage of the proposed method. The p and q norm values at different iteration steps are illustrated in Fig. 11. Here, it can be seen that the norm values are stable after a certain number of iterations. For the q maps, smaller norms assigned to edge regions, and larger norms corresponding to the smooth regions.

In order to validate the universality of the proposed adaptive method, it was tested using eight additional images of different types, as shown in Fig. 12. The mixed noise (Gaussian variance $= 0.001$, impulse density $= 0.1$) was considered in this experiment. The quantitative results are shown in Table VI. Here, it can be seen that the most commonly employed model

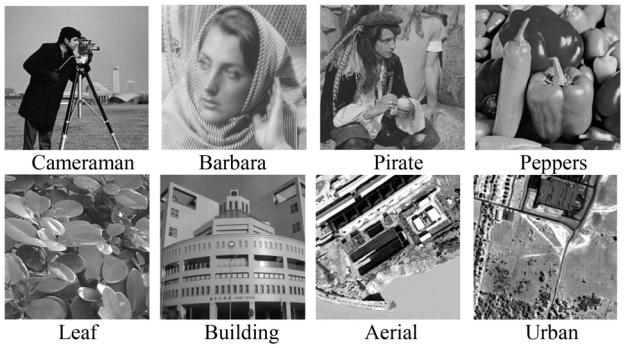

Fig. 12. Eight images for the validation of the proposed adaptive method.

TABLE VI
PSNR RESULTS OF THE EXPERIMENTS PERFORMED ON THE DIFFERENT IMAGES

	Cameraman	Barbara	Pirate	Peppers	Leaf	Building	Aerial	Urban
l_2 + IRTV	26.165	24.742	25.816	27.697	26.083	26.944	23.791	23.056
l_1 + IRTV	29.394	28.292	28.247	30.622	29.258	30.186	27.015	25.460
l_1 + ANA	29.518	28.363	28.258	30.748	29.364	30.226	27.149	25.543
l_1 + SWTV	29.606	28.490	28.360	30.846	29.519	30.399	27.520	25.622
Proposed	30.084	28.784	28.741	31.366	30.176	30.893	27.903	26.011

(l_2 + IRTV) produces very poor results because of the inapplicability of the l_2 fidelity to impulse noise. When the l_2 fidelity is replaced by the l_1 fidelity, the results are greatly improved. If we replace the standard TV model by the ANA and SWTV regularization models, the PSNR values can be further increased. Finally, when compared with the different combinations of the existing fidelity and regularization models, the proposed method produces the highest quantitative evaluation results.

D. Discussion of the Proposed Method

1) Parameter Analysis: There are two main parameters that can affect the results. The first is the shape controller parameter α in (25). By tuning α from 0 to 1.0, different results can be acquired. However, the parameter selection is always a headache for image processing. In Fig. 13, we give the results of synthetic experiments with the *Lena* and *Cameraman* images (contaminated with Gaussian noise with variance of 0.001) for SR. Here, it can be seen that the results are not very sensitive to the hyper-parameter α. Based on a large amount of tests, we fixed α as 0.5 in all the experiments.

The other significant parameter is the regularization parameter λ. This differs in accordance with the content of the image and the noise level. In general, the regularization parameter λ has a very important effect on the resulting image. Although there have been some methods developed to determine this parameter adaptively [14], [50], [51], only approximate optimal solutions can be obtained in most cases. In our experiments, the main aim is to prove the advantages of the proposed adaptive norms. If the above methods for selecting regularization parameter are used, it will bring great uncertainties for the comparison between the proposed and the traditional methods. Therefore, for a fair comparison between different models, the regularization parameter was manually determined by attempting a series of values and selecting the one with the highest PSNR (in simulated experiments) or the best visual effect (in real experiments).

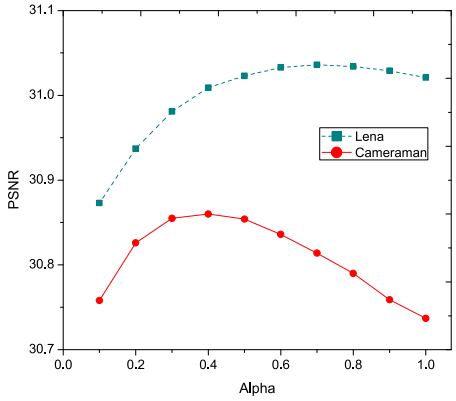

Fig. 13. PSNR (dB) with different values of α.

2) Convergence Discussion: As described before, this paper employs the IRLS method and the LDFPI method for the linearization of the fidelity term and the regularization term, respectively. The convergence of the two optimization methods for l_p norm problems has been proved in [35] and [37], in which the norm values were fixed. We also confirmed that the norms converge to stable values after a certain number of iterations, as shown in Fig. 11. To further validate the convergence behavior, Fig. 14 illustrates the PSNR values, relative residuals $||z_n - z_{n-1}||_2^2/||z_n||_2^2$, and objective function values $E_n(z)$ versus the iteration number in the *Lena* SR experiment, in which both fidelity and regularization norms were adaptively solved. In order to test the sensitivity to the initial guess, two curves corresponding to zero initialization and bilinear interpolation initialization are illustrated in each figure. Here, it can be seen that the residuals and objective function values decrease with the iteration, and the PSNR values become very stable values after a few iterative steps. More importantly, although the two initial conditions have great differences, their corresponding curves are almost overlapped in the latter part of the iteration. All of these factors indicate that the proposed method has a good convergence behavior.

3) Computational Efficiency: In this section, we give an example of the running time of the proposed method (Fig. 15). The size of the reconstructed image is 256 × 256, and the method was implemented on a common notebook computer with an Intel Core i7 1.90 GHz CPU and 8 GB of internal memory. We can see that the proposed method is very efficient in the Gaussian noise case, but it needs more time in the impulse noise case. The mixed case falls in between the two pure cases. In fact, when the proportion of impulse noise is large, the optimal norm value would be smaller and the running time would be increased. In Fig. 15, the traditional TV SR method (with l_2-norm fidelity in the Gaussian case and l_1-norm fidelity in the impulse and mixed cases) is used for contrast, and it can be seen the procedure for the adaptive selection of norms does not considerably increase the running time. Furthermore, the proposed l_p+l_q method is more efficient than the traditional l_1 + TV method in the mixed case.

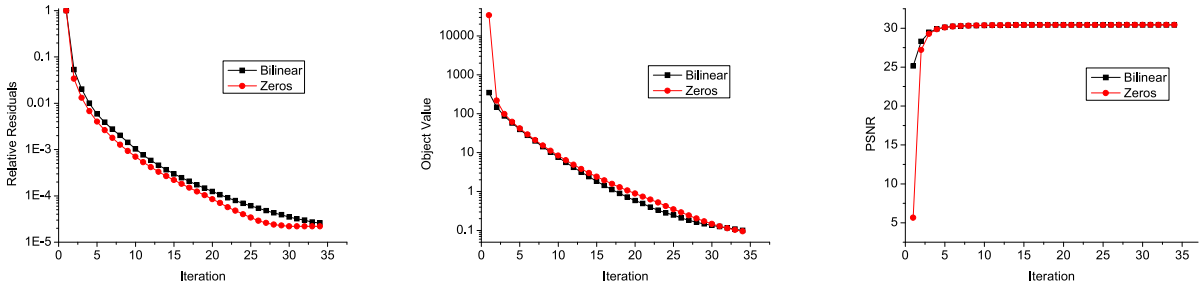

Fig. 14. Convergence of the proposed method by comparing zero initialization and bilinear interpolation initialization for *Lena* image in mixed noise case (variance = 0.001, density = 0.01). (a) Relative residuals. (b) Objective function values. (c) PSNR values.

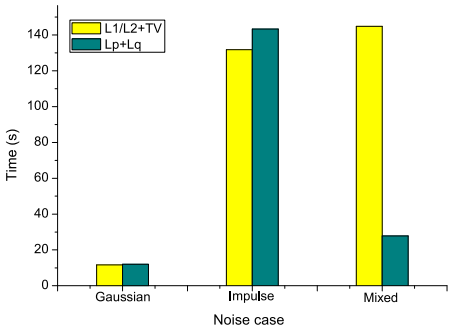

Fig. 15. Running time of the proposed method.

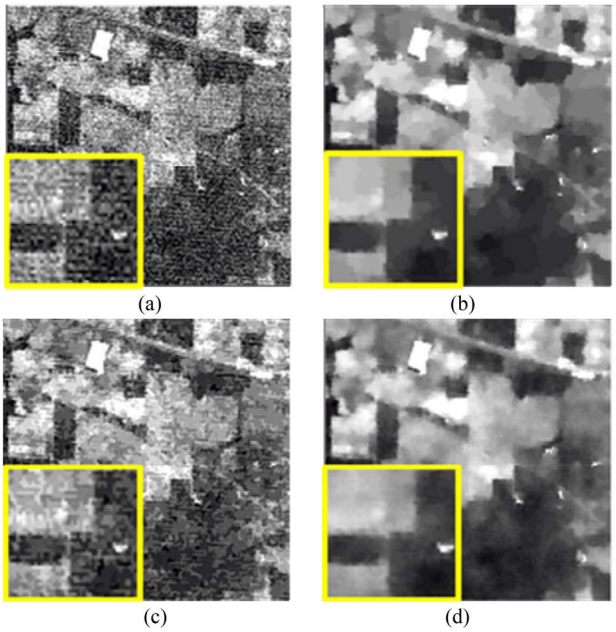

Fig. 16. Results for the Indian Pines dataset in the first real experiment. (a) Original noisy image. (b)–(d) Results for l_2 + TV, l_1 + TV, and the proposed method, respectively.

4) Experiments With Real Images: To verify the performance of the proposed method on real data, we conducted two experiments for restoration and SR, respectively. The first restoration experiment involved the 2nd band of the Airborne Visible InfraRed Imaging Spectrometer Indian Pines dataset, which is a hyperspectral image with 220 bands. The test data with the size of 145×145 pixels are shown in Fig. 16(a).

Fig. 17. Results for the compressed face sequence in the second real data experiment. (a) Original noisy image (b)–(d) Results for l_2+TV, l_1+TV, and the proposed method, respectively.

From the figure, we can see that this image is severely contaminated by noise, and the noise type is complex. The restoration is a difficult task as the noise model is complex and difficult to identify. The results of the proposed method, as well as the original noisy image and the results for the l_1/l_2 fidelity norm with TV regularization are shown in Fig. 16. It is known that any denoising algorithm inevitably removes some detailed information more or less when removing the noise. However, the denoised image often has better overall visual quality. From the visual effect, it can be seen that the l_2+TV method [Fig. 16(b)] results in a staircase effect when removing the noise. Meanwhile, the l_2 + TV method [Fig. 16(c)] cannot effectively remove the noise because the noise distribution is approximately Gaussian. The proposed method performs well at preserving the texture and eliminating the staircase effect, while also removing noise.

The second SR experiment was conducted on the Face sequence, with ten compressed images following the global translational motion model. The data size was 32×31,

and the magnification factor was set as four. The corresponding results are presented in Fig. 17. Here, the difference between the results can be clearly seen. Due to the compressed effects, the noise model in the images is actually not pure Gaussian. Therefore, the proposed method outperforms the $l_2 + \text{TV}$ and $l_1 + \text{TV}$ methods. In the results of the proposed method, the edges are well reconstructed and the compressed staircase effect is effectively suppressed.

V. Conclusion

In this paper, we have proposed an adaptive method to determine the norms in a regularized (SR) restoration model. Two norm functions are deduced from different viewpoints, respectively, for the fidelity term and the regularization term. The adaptation of the fidelity term ($l_{a,p}$) is to ensure that the method is robust in different noise types (Gaussian, impulse, or mixed). The target of the adaptive regularization norm ($l_{a,q}$) is to ensure that not only that the edge information is enhanced, but that the smooth regions do not give rise to artifacts such as staircase effects. The experimental results confirm that the two proposed norm functions are both very promising. In fact, these two functions can be used independently or jointly because they are aimed at different problems. The $l_{a,p}$ norm fidelity is effective in situations where the noise statistics are unknown. The $l_{a,q}$ norm regularization can improve the results in any type of noise case. Especially when the noise is strong, the proposed method still has good performance. Nevertheless, there may still be room for considerable improvement of the proposed method. For example, other functional forms of the fidelity and regularization norms could be attempted under the framework of this paper. Another possible but challenging issue would be to seek an adaptive method for the optimal determination of α, as an alternative to the compromised setting in the regularization norm function. It will also be important to give mathematical convergence proof of the proposed method.

References

[1] J.-H. Wang, W.-J. Liu, and L.-D. Lin, "Histogram-based fuzzy filter for image restoration," *IEEE Trans. Syst., Man, Cybern. B, Cybern.*, vol. 32, no. 2, pp. 230–238, Apr. 2002.

[2] B. J. Kang and K. R. Park, "Real-time image restoration for iris recognition systems," *IEEE Trans. Syst., Man, Cybern. B, Cybern.*, vol. 37, no. 6, pp. 1555–1566, Dec. 2007.

[3] R. Yan, L. Shao, L. Liu, and Y. Liu, "Natural image denoising using evolved local adaptive filters," *Signal Process.*, vol. 103, pp. 36–44, Oct. 2014.

[4] H. Shen, W. Zhao, Q. Yuan, and L. Zhang, "Blind restoration of remote sensing images by a combination of automatic knife-edge detection and alternating minimization," *Remote Sens.*, vol. 6, no. 8, pp. 7491–7521, 2014.

[5] S. C. Park, M. K. Park, M. G. Kang, "Super-resolution image reconstruction: A technical overview," *IEEE Signal Process. Mag.*, vol. 20, no. 3, pp. 21–36, May 2003.

[6] H. Shen, L. Zhang, B. Huang, and P. Li, "A MAP approach for joint motion estimation, segmentation, and super resolution," *IEEE Trans. Image Process.*, vol. 16, no. 2, pp. 479–490, Feb. 2007.

[7] S. Farsiu, D. Robinson, M. Elad, and P. Milanfar, "Advances and challenges in super-resolution," *Int. J. Imag. Syst. Technol.*, vol. 14, no. 2, pp. 47–57, 2004.

[8] S. Baker and T. Kanade, "Limits on super-resolution and how to break them," *IEEE Trans. Pattern Anal. Mach. Intell.*, vol. 24, no. 9, pp. 1167–1183, Sep. 2002.

[9] J. Tian and K.-K. Ma, "A survey on super-resolution imaging," *Signal Image Video Process.*, vol. 5, no. 3, pp. 329–342, 2011.

[10] K. Nasrollahi and T. B. Moeslund, "Super-resolution: A comprehensive survey," *Mach. Vis. Appl.*, vol. 25, no. 6, pp. 1423–1468, 2014.

[11] M. K. Ng, H. Shen, L. Zhang, and E. Lam, "A total variation based super-resolution reconstruction algorithm for digital video," *EURASIP J. Adv. Signal Process.*, vol. 2007, Jun. 2007, Art. ID 74585.

[12] D. Bertaccini, R. Chan, S. Morigi, and F. Sgallari, "An adaptive norm algorithm for image restoration," in *Proc. Scale Space Variat. Methods Comput. Vis.*, Ein Gedi, Israel, 2012, pp. 194–205.

[13] R. R. Schultz and R. L. Stevenson, "Extraction of high-resolution frames from video sequences," *IEEE Trans. Image Process.*, vol. 5, no. 6, pp. 996–1011, Jun. 1996.

[14] E. S. Lee and M. G. Kang, "Regularized adaptive high-resolution image reconstruction considering inaccurate subpixel registration," *IEEE Trans. Image Process.*, vol. 12, no. 7, pp. 826–837, Jul. 2003.

[15] H. Zhang, J. Yang, Y. Zhang, and T. S. Huang, "Image and video restorations via nonlocal kernel regression," *IEEE Trans. Cybern.*, vol. 43, no. 3, pp. 1035–1046, Jun. 2013.

[16] S. Farsiu, D. Robinson, M. Elad, and P. Milanfar, "Robust shift and add approach to super-resolution," *Proc. SPIE Int. Soc. Opt. Eng.*, vol. 5203, pp. 121–130, Nov. 2003.

[17] S. Farsiu, M. D. Robinson, M. Elad, and P. Milanfar, "Fast and robust multiframe super resolution," *IEEE Trans. Image Process.*, vol. 13, no. 10, pp. 1327–1344, Oct. 2004.

[18] Y. Dong, M. Hintermüller, and M. Neri, "A primal-dual method for L1 TV image denoising," *SIAM J. Imag. Sci.*, vol. 2, no. 4, pp. 1168–1189, 2009.

[19] R. H. Chan, Y. Dong, and M. Hintermüller, "An efficient two-phase L1-TV method for restoring blurred images with impulse noise," *IEEE Trans. Image Process.*, vol. 19, no. 7, pp. 1731–1739, Jul. 2010.

[20] T. F. Chan and S. Esedoglu, "Aspects of total variation regularized L1 function approximation," *SIAM J. Appl. Math.*, vol. 65, no. 5, pp. 1817–1837, 2005.

[21] X. L. Li, Y. W. Pang, and Y. A. Yuan, "L1-norm-based 2DPCA," *IEEE Trans. Syst., Man, Cybern. B, Cybern.*, vol. 40, no. 4, pp. 1170–1175, Aug. 2010.

[22] H. F. Shen, M. K. Ng, P. X. Li, and L. P. Zhang, "Super resolution reconstruction algorithm to MODIS remote sensing images," *Comput. J.*, vol. 52, no. 1, pp. 90–100, 2009.

[23] H. Fu, M. K. Ng, M. Nikolova, and J. L. Barlow, "Efficient minimization methods of mixed l1-l1 and l2-l1 norms for image restoration," *SIAM J. Sci. Comput.*, vol. 27, no. 6, pp. 1881–1902, 2006.

[24] Y.-R. Li and D.-Q. Dai, "Color superresolution reconstruction and demosaicing using elastic net and tight frame," *IEEE Trans. Circuits Syst. I, Reg. Papers*, vol. 55, no. 11, pp. 3500–3512, Dec. 2008.

[25] O. A. Omer and T. Tanaka, "Region-based weighted-norm approach to video super-resolution with adaptive regularization," in *Proc. IEEE Int. Conf. Acoust. Speech Signal Process.*, Taipei, Taiwan, 2009, pp. 833–836.

[26] S. Huihui, Z. Lei, and W. Peikang, "An adaptive l1-l2 hybrid error model to super-resolution," in *Proc. IEEE Int. Conf. Image Process.*, Hong Kong, 2010, pp. 2821–2824.

[27] X. Zhang, E. Y. Lam, E. X. Wu, and K. K. Y. Wong, "Application of Tikhonov regularization to super-resolution reconstruction of brain MRI images," in *Medical Imaging and Informatics*. Berlin, Germany: Springer, 2008, pp. 51–56.

[28] J.-S. Lee and C. H. Park, "Hybrid simulated annealing and its application to optimization of hidden Markov models for visual speech recognition," *IEEE Trans. Syst., Man, Cybern. B, Cybern.*, vol. 40, no. 4, pp. 1188–1196, Aug. 2010.

[29] M. K. Ng, H. Shen, S. Chaudhuri, and A. C. Yau, "Zoom-based super-resolution reconstruction approach using prior total variation," *Opt. Eng.*, vol. 46, no. 12, 2007, Art. ID 127003.

[30] Q. Yuan, L. Zhang, and H. Shen, "Multiframe super-resolution employing a spatially weighted total variation model," *IEEE Trans. Circuits Syst. Video Technol.*, vol. 22, no. 3, pp. 379–392, Mar. 2012.

[31] L. Zhang, Q. Yuan, H. Shen, and P. Li, "Muti-frame image super-resolution adapted with local spatial information," *J. Opt. Soc. America A*, vol. 28, no. 3, pp. 381–390, 2011.

[32] L. Zhang, H. Zhang, H. Shen, and P. Li, "A super-resolution reconstruction algorithm for surveillance images," *Signal Process.*, vol. 90, no. 3, pp. 848–859, 2010.

[33] L. Zhang, H. Shen, W. Gong, and H. Zhang, "Adjustable model-based fusion method for multispectral and panchromatic images," *IEEE Trans. Syst., Man, Cybern. B, Cybern.*, vol. 42, no. 6, pp. 1693–1704, Dec. 2012.

[34] L. Yue, H. Shen, Q. Yuan, and L. Zhang, "A locally adaptive L1-L2 norm for multi-frame super-resolution of images with mixed noise and outliers," *Signal Process.*, vol. 105, pp. 156–174, Dec. 2014.
[35] P. Rodrguez and B. Wohlberg, "Efficient minimization method for a generalized total variation functional," *IEEE Trans. Image Process.*, vol. 18, no. 2, pp. 322–332, Feb. 2009.
[36] R. Wolke and H. Schwetlick, "Iteratively reweighted least squares: Algorithms, convergence analysis, and numerical comparisons," *SIAM J. Sci. Statist. Comput.*, vol. 9, no. 5, pp. 907–921, 1988.
[37] C. Vogel and M. E. Oman, "Iterative methods for total variation denoising," *SIAM J. Sci. Comput.,* vol. 17, no. 1, pp. 227–238, 1996.
[38] F.-R. Lin, M. K. Ng, and W.-K. Ching, "Factorized banded inverse preconditioners for matrices with Toeplitz structure," *SIAM J. Sci. Comput.*, vol. 26, no. 6, pp. 1852–1870, 2005.
[39] R. Yan, L. Shao, and Y. Liu, "Nonlocal hierarchical dictionary learning using wavelets for image denoising," *IEEE Trans. Image Process.*, vol. 22, no. 12, pp. 4689–4698, Dec. 2013.
[40] L. Shao, R. Yan, X. Li, and Y. Liu, "From heuristic optimization to dictionary learning: A review and comprehensive comparison of image denoising algorithms," *IEEE Trans. Cybern.*, vol. 44, no. 7, pp. 1001–1013, Jul. 2008.
[41] M. E. Zervakis and A. N. Venetsanopoulos, "Linear and nonlinear image restoration under the presence of mixed noise," *IEEE Trans. Circuits Syst.*, vol. 38, no. 3, pp. 258–272, Mar. 1991.
[42] J.-F. Cai, R. H. Chan, and M. Nikolova, "Two-phase approach for deblurring images corrupted by impulse plus Gaussian noise," *Invers. Prob. Imag.*, vol. 2, no. 2, pp. 187–204, 2008.
[43] S. K. Mitra and G. Sicuranza, *Nonlinear Image Processing*. Burlington, MA, USA: Elsevier, 2000.
[44] K.-S. Song, "A globally convergent and consistent method for estimating the shape parameter of a generalized Gaussian distribution," *IEEE Trans. Inf. Theory*, vol. 52, no. 2, pp. 510–527, Feb. 2006.
[45] J. Bigun and G. H. Granlund, "Optimal orientation detection of linear symmetry," in *Proc. 1st Int. Conf. Comput. Vis.*, London, U.K., 1987, pp. 433–438.
[46] T. Brox, J. Weickert, B. Burgeth, and P. Mrázek, "Nonlinear structure tensors," *Image Vis. Comput.*, vol. 24, no. 1, pp. 41–55, 2006.
[47] Y. Wang, R. Niu, L. Zhang, and H. Shen, "Region-based adaptive anisotropic diffusion for image enhancement and denoising," *Opt. Eng.*, vol. 49, no. 11, 2010, Art. ID 117007.
[48] T. Brox, M. Rousson, R. Deriche, and J. Weickert, "Colour, texture, and motion in level set based segmentation and tracking," *Image Vis. Comput.*, vol. 28, no. 3, pp. 376–390, 2010.
[49] X.-F. Wang, D.-S. Huang, and H. Xu, "An efficient local Chan–Vese model for image segmentation," *Pattern Recognit.*, vol. 43, no. 3, pp. 603–618, 2010.
[50] Q. Yuan, L. Zhang, H. Shen, and P. Li, "Adaptive multiple-frame image super-resolution based on U-curve," *IEEE Trans. Image Process.*, vol. 19, no. 12, pp. 3157–3170, Dec. 2010.
[51] N. K. Bose, S. Lertrattanapanich, and J. Koo, "Advances in superresolution using L-curve," in *Proc.IEEE Int. Symp. Circuits Syst.*, vol. 2. Sydney, NSW, Australia, 2001, pp. 433–436.

Huanfeng Shen (M'11–SM'13) received the B.S. degree in surveying and mapping engineering and the Ph.D. degree in photogrammetry and remote sensing from Wuhan University, Wuhan, China, in 2002 and 2007, respectively.

In 2007, he was with the School of Resource and Environmental Sciences, Wuhan University, where he was a Luojia Distinguished Professor. His current research interests include image quality improvement, remote sensing mapping and application, data fusion and assimilation, and regional and global environmental change. He has published over 100 research papers. He has been supported by several talent programs, such as the China National Science Fund for Excellent Young Scholars 2014, the New Century Excellent Talents by the Ministry of Education of China 2011, the Hubei Science Fund for Distinguished Young Scholars 2011.

Dr. Shen serves as a Council Member for the China Association of Remote Sensing Application. He is currently a member of the Editorial Board of *Journal of Applied Remote Sensing*.

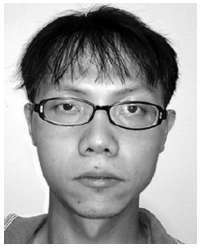

Li Peng received the B.S. degree in geographic information system and the M.S degree in surveying and mapping engineering from Wuhan University, Wuhan, China in 2010 and 2012, respectively.

Since 2010, he has been focused on image recovery and super resolution. In 2012 and 2013, he was dedicated in designing applicable fusion and super resolution algorithms for Satellite images. He is currently a Web Application Developer and is Acute to Geolocations and Maps.

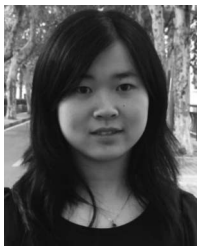

Linwei Yue received the B.S. degree in geographic information system from Wuhan University, Wuhan, China, in 2012. She is currently pursuing the Ph.D. degree with the State Key Laboratory of Information Engineering in Surveying Mapping and Remote Sensing, Wuhan University.

Her current research interests include image super-resolution, DEM accuracy enhancement, and data fusion.

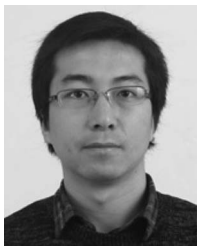

Qiangqiang Yuan (M'14) received the B.S. degree in surveying and mapping engineering and the Ph.D. degree in photogrammetry and remote sensing from Wuhan University, Wuhan, China, in 2006 and 2012, respectively.

He was with the School of Geodesy and Geomatics, Wuhan University, in 2012, where he is currently an Associate Professor. He has served as a Referee for over ten international journals for remote sensing and image processing. His current research interests include image reconstruction, remote sensing image processing and application, and data fusion.

Dr. Yuan was a recipient of the Top-Ten Academic Star of Wuhan University in 2011, the Hong Kong Scholar Award from the Society of Hong Kong Scholars and the China National Post-Doctoral Council in 2014.

Liangpei Zhang (M'06–SM'08) received the B.S. degree in physics from Hunan Normal University, ChangSha, China, in 1982, and the M.S. degree in optics from the Xi'an Institute of Optics and Precision Mechanics of Chinese Academy of Sciences, Xi'an, China, in 1988, and the Ph.D. degree in photogrammetry and remote sensing from Wuhan University, Wuhan, China, in 1998.

He is currently the Head of the Remote Sensing Division, State Key Laboratory of Information Engineering in Surveying, Mapping and Remote Sensing, Wuhan University. He is also a Chang-Jiang Scholar Chair Professor with the Ministry of Education of China, Beijing, China. Since 2011, he has been a Principal Scientist for the China State Key Basic Research Project appointed by the Ministry of National Science and Technology of China to lead the remote sensing program in China. His current research interests include hyperspectral remote sensing, high-resolution remote sensing, image processing, and artificial intelligence. He has over 410 research papers and holds 15 patents.

Dr. Zhang was a recipient of the 2010 Best Paper Boeing Award and the 2013 Best Paper ERDAS Award of American Society of Photogrammetry and Remote Sensing, respectively. He is a Fellow of the Institution of Engineering and Technology, an Executive Member (Board of Governor) of the China National Committee of the International Geosphere-Biosphere Programme, and an Executive Member of the China Society of Image and Graphics. He serves as a Co-Chair for the series SPIE Conferences on Multispectral Image Processing and Pattern Recognition, Conference on Asia Remote Sensing, and many other conferences. He is an Editor several conference proceedings, issues, and geoinformatics symposiums. He also serves as an Associate Editor of the *International Journal of Ambient Computing and Intelligence*, the *International Journal of Image and Graphics*, the *International Journal of Digital Multimedia Broadcasting*, the *Journal of Geo-Spatial Information Science*, the *Journal of Remote Sensing*, and the IEEE TRANSACTIONS ON GEOSCIENCE AND REMOTE SENSING.